Int J Thermophys (2009) 30:2122–2143
DOI 10.1007/s10765-009-0652-9

Elastodynamic Behavior of Waves in Thermo-Microstretch Elastic Plate Bordered with Layers of Inviscid Liquid

Rajneesh Kumar · Geeta Partap

Received: 8 November 2008 / Accepted: 16 September 2009 / Published online: 4 December 2009

Abstract The elastodynamic behavior of waves in a thermo-microstretch elastic homogeneous isotropic plate bordered with layers of inviscid liquid on both sides subjected to stress-free thermally insulated and isothermal conditions is investigated in the context of Lord and Shulman and Green and Lindsay theories of thermoelasticity. The mathematical model has been simplified by using the Helmholtz decomposition technique, and the frequency equations for different mechanical situations are obtained and discussed. The special cases such as short wavelength waves and regions of the secular equations are also discussed. Finally, the numerical solution is carried out for a magnesium crystal composite material plate bordered with water. The dispersion curves, attenuation coefficients, amplitudes of dilatation, microrotation, microstretch, and temperature distribution for the symmetric and skew-symmetric wave modes are presented graphically.

Keywords Attenuation coefficient · Inviscid liquid · Microstretch · Phase velocity · Secular equations

R. Kumar
Department of Mathematics, Kurukshetra University, Kurukshetra, Haryana 136 119, India
e-mail: rajneesh_kuk@rediffmail.com

G. Partap (✉)
Department of Mathematics, Dr. B. R. Ambedkar National Institute of Technology, Jalandhar, Punjab 144 011, India
e-mail: pratapg@nitj.ac.in; gp.recjal@gmail.com

1 Introduction

The theory of microstretch elastic solids has been introduced by Eringen [1–3]. This theory is a special case of the micromorphic theory. In the framework of micromorphic theory, a material point is endowed with three deformable directors. When the directors are constrained to have only breathing-type microdeformations, then the body is a microstretch continuum [3]. The material points of these continua can stretch and contract independently of their translations and rotations. The theory is expected to find applications in the treatment of the mechanics of composite materials reinforced with chopped fibers and various porous materials. Theory of microstretch continua is a generalization of the theory of micropolar continua.

Eringen [2] developed the theory of thermo-microstretch elastic solids. Eringen [4] also derived the equations of motions, constitutive equations, and boundary conditions for thermo-microstretch fluids and obtained the solution of the problem for acoustical waves in bubbly liquids. A microstretch continuum is a model for a Bravais lattice with its basis on the atomic level and two-phase dipolar solids with a core on the macroscopic level. Composite materials reinforced with chopped elastic fibers, porous media whose pores are filled with gas or inviscid liquid, asphalt, or other elastic inclusions and solid–liquid crystals, etc., are examples of microstretch solids.

During the last four decades, wide spread attention has been given to thermoelasticity theories which admit a finite speed for the propagation of a thermal field. Lord and Shulman [5] reported a new theory based on a modified Fourier's Law of heat conduction with one relaxation time. A more rigorous theory of thermoelasticity by introducing two relaxation times has been formulated by Green and Lindsay (G-L) [6].

Schoch [7] investigated the effect of an inviscid liquid on the propagation of Lamb waves. When a plate of finite thickness is bordered with a half-space homogeneous liquid on both sides, part of the Lamb wave energy in the plate is coupled into the liquid as radiation; most of the energy is still in the solid. This type of disturbance is called the leaky Lamb wave. Schoch derived the dispersion relations for leaky Lamb waves for an isotropic plate and an inviscid liquid.

For a thin plate, the zeroth-order anti-symmetrical mode (a_0 mode) Lamb wave is often called the flexural or bending wave. Kurtze and Bolt [8] derived a dispersion equation for bending waves when a plate is in contact with inviscid fluid based on the acoustic impedance concept. Watkins et al. [9] calculated the attenuation of Lamb waves in the presence of an inviscid liquid using an acoustic impedance method. Wu and Zhu [10] studied the propagation of Lamb waves in a plate bordered with an inviscid liquid layer on both sides. The dispersion equations of this case were derived and solved numerically. Zhu and Wu [11] derived the dispersion equations of the Lamb waves of a plate bordered with a viscous liquid layer or half-space viscous liquid on both sides. Sharma et al. [12,13] derived the dispersion equations of Lamb waves in homogeneous isotropic and transversely isotropic thermoelastic plate bordered with an inviscid liquid layer or half-space on both sides.

The aim of this article is to study the elastodynamic behavior of waves in an infinite homogeneous isotropic thermo-microstretch elastic plate of thickness $2d$ bordered with a layer of inviscid liquid on both sides in the context of generalized theories of thermoelasticity.

2 Basic Equations

The equations of motion and the constitutive relations in a homogeneous isotropic thermo-microstretch elastic solid in the absence of body forces, body couples, stretch force, and heat sources are given by Eringen [3], Lord and Shulman [5], and Green and Lindsay [6].

$$(\lambda+2\mu+K)\nabla(\nabla\cdot\vec{u})-(\mu+K)\nabla\times\nabla\times\vec{u}+K\nabla\times\vec{\varphi} -\nu\left(1+\tau_1\tfrac{\partial}{\partial t}\right)\nabla T+\lambda_0\nabla\varphi^*=\rho\tfrac{\partial^2\vec{u}}{\partial t^2}, \tag{1}$$

$$(\alpha+\beta+\gamma)\nabla(\nabla\cdot\vec{\varphi})-\gamma\nabla\times(\nabla\times\vec{\varphi})+K\nabla\times\vec{u}-2K\vec{\varphi}=\rho j\tfrac{\partial^2\vec{\varphi}}{\partial t^2}, \tag{2}$$

$$\alpha_0\nabla^2\varphi^*+\nu_1\left(T+\tau_1\tfrac{\partial T}{\partial t}\right)-\lambda_1\varphi^*-\lambda_0\nabla\cdot\vec{u}=\tfrac{\rho j_0}{2}\tfrac{\partial^2\varphi^*}{\partial t^2}, \tag{3}$$

$$K^*\nabla^2T=\rho C^*\left(\tfrac{\partial T}{\partial t}+\tau_0\tfrac{\partial^2T}{\partial t^2}\right) +\nu T_0\left(\tfrac{\partial}{\partial t}+\eta_0\tau_0\tfrac{\partial^2}{\partial t^2}\right)(\nabla\cdot\vec{u})+\nu_1T_0\left(\tfrac{\partial}{\partial t}+\eta_0\tau_0\tfrac{\partial^2}{\partial t^2}\right)\varphi^*, \tag{4}$$

$$t_{ij}=\lambda u_{r,r}\delta_{ij}+\mu(u_{i,j}+u_{j,i})+K(u_{j,i}-\varepsilon_{ijr}\varphi_r)-\nu\left(T+\tau_1\tfrac{\partial T}{\partial t}\right)\delta_{ij} +\lambda_0\delta_{ij}\varphi^*, \tag{5}$$

$$m_{ij}=\alpha\varphi_{r,r}\delta_{ij}+\beta\varphi_{i,j}+\gamma\varphi_{j,i}+b_0\varepsilon_{mji}\varphi^*_{,m},\quad \lambda^*_i=\alpha_0\varphi^*_{,i}+b_0\varepsilon_{ijm}\varphi_{j,m}, \tag{6}$$

where $\lambda, \mu, \alpha, \beta, \gamma, K, \alpha_0, \lambda_0, \lambda_1$, and b_0 are material constants, ρ is the density, j is the microinertia, j_0 is the microinertia of microelements, t_{ij} and m_{ij} are the components of stress and couple stress tensors, respectively, $\vec{u}=(u_r,u_\theta,u_z)$ is the displacement vector, $\vec{\varphi}=(\varphi_r,\varphi_\theta,\varphi_z)$ is the microrotation vector, φ^* is the scalar point microstretch function, λ^*_i is the microstress tensor, T is the temperature change, T_0 is a uniform temperature, $\nu=(3\lambda+2\mu+K)\alpha_{t_1}$, $\nu_1=(3\lambda+2\mu+K)\alpha_{t_2}$, α_{t_1}, and α_{t_2} are the coefficients of linear thermal expansion, K^* is the coefficient of thermal conductivity, C^* is the specific heat at constant strain, and δ_{ij} is the Kronecker delta. The comma notation denotes spatial derivatives.

3 Formulation of the Problem

We consider an infinite homogeneous isotropic, thermally conducting microstretch elastic plate of thickness $2d$ initially at a uniform temperature T_0. The plate is bordered both on the top and bottom with homogeneous inviscid liquid layers of thickness h (if $h\to\infty$, it becomes the leaky Lamb wave-type case). The plate is axi-symmetric with respect to the z-axis as the axis of symmetry. The circular cylindrical coordinates (r,θ,z) have been used to describe the response of the plate. The origin of the co-ordinate system (r,θ,z) is taken at any point in the middle surface of the plate and the z-axis normal to it along the thickness. We take the r–z plane as the plane of incidence.

For a two-dimensional problem, we take

$$\vec{u}=(u_r,0,u_z),\quad \vec{\varphi}=(0,\varphi_\theta,0),\quad \text{and } \vec{u}_{\mathrm{L}}=(u_{\mathrm{L}},0,w_{\mathrm{L}}). \tag{7}$$

We define the dimensionless quantities,

$$r' = \frac{\omega^* r}{c_1}, \quad z' = \frac{\omega^* z}{c_1}, \quad u_r' = \frac{\rho\omega^* c_1}{\nu T_0} u_r, \quad u_z' = \frac{\rho\omega^* c_1}{\nu T_0} u_z, \quad t' = \omega^* t,$$
$$\varphi_\theta' = \frac{\rho c_1^2}{\nu T_0}\varphi_\theta, \varphi^{*'} = \frac{\rho c_1^2}{\nu T_0}\varphi^*, T' = \frac{T}{T_0}, \quad \tau_1' = \omega^*\tau_1$$
$$\tau_0' = \omega^*\tau_0, \quad t_{ij}' = \frac{1}{\nu T_0} t_{ij}, \quad m_{ij}' = \frac{\omega^* m_{ij}}{c_1 \nu T_0}, \quad h' = \frac{c_1 h}{\omega^*}, \quad p = \frac{K}{\rho c_1^2},$$
$$p_1 = \frac{\lambda_1}{\rho c_1^2}, \quad p_0 = \frac{\lambda_0}{\rho c_1^2}, \quad \delta^2 = \frac{c_2^2}{c_1^2}, \quad \delta_1^2 = \frac{c_3^2}{c_1^2},$$
$$\delta_2^2 = \frac{c_4^2}{c_1^2}, \quad c_\mathrm{L}^2 = \frac{\lambda_\mathrm{L}}{\rho_\mathrm{L}}, \quad \delta_\mathrm{L}^2 = \frac{c_\mathrm{L}^2}{c_1^2}, \quad \bar{\nu} = \frac{\nu_1}{\nu}, \quad u_\mathrm{L}' = \frac{\rho_\mathrm{L}\omega^* c_1}{\nu T_0} u_\mathrm{L},$$
$$w_\mathrm{L}' = \frac{\rho_\mathrm{L}\omega^* c_1}{\nu T_0} w_\mathrm{L}, \quad \delta^{*^2} = \frac{K c_1^2}{\gamma\omega^*}, \quad \delta_1^* = \frac{\rho c_1^4}{\alpha_0 \omega^{*^2}},$$
$$\omega^* = \frac{\rho C^* c_1^2}{K^*}, \quad \lambda_i^{*'} = \frac{\lambda_i^* \omega^*}{c_1 \nu T_0}, \tag{8}$$

where $c_1^2 = \frac{\lambda+2\mu+K}{\rho}$, $c_2^2 = \frac{\mu+K}{\rho}$, $c_3^2 = \frac{\gamma}{\rho j}$, $c_4^2 = \frac{2\alpha_0}{\rho j_0}$, $\in = \frac{\nu^2 T_0}{\rho^2 C^* c_1^2}$, ω^* is the characteristic frequency of the medium, c_L is the velocity of sound in the liquid, ρ_L is the density of the liquid, λ_L is the bulk modulus, and $\in$ is the thermoelastic coupling constant.

For the liquid half-space, the equation of motion and constitutive relation are given by

$$\lambda_\mathrm{L}\nabla(\nabla.\vec{u}_\mathrm{L}) = \rho_\mathrm{L}\frac{\partial^2\vec{u}_\mathrm{L}}{\partial t^2}, \tag{9}$$
$$\left(t_{ij}\right)_\mathrm{L} = \lambda_\mathrm{L}(u_{r,r})_\mathrm{L}\delta_{ij}. \tag{10}$$

In the solid, we introduce the potential functions φ and ψ through the relations,

$$u_r = \frac{\partial\varphi}{\partial r} + \frac{\partial\psi}{\partial z}, \quad u_z = \frac{\partial\varphi}{\partial z} - \frac{\partial\psi}{\partial r} - \frac{\psi}{r}, \tag{11}$$

where φ and ψ are the velocity potential functions of longitudinal and shear waves.

In the liquid boundary layers, we have

$$u_{\mathrm{L}_i} = \frac{\partial\varphi_{\mathrm{L}_i}}{\partial r} + \frac{\partial\psi_{\mathrm{L}_i}}{\partial z} \quad \text{and} \quad w_{\mathrm{L}_i} = \frac{\partial\varphi_{\mathrm{L}_i}}{\partial z} - \frac{\partial\psi_{\mathrm{L}_i}}{\partial r} - \frac{\psi_{\mathrm{L}_i}}{r}, \quad i = 1, 2, \tag{12}$$

where φ_{L_i} and ψ_{L_i} are, respectively, the scalar velocity potential and vector velocity component along the θ-direction, for the top liquid layer ($i = 1$) and for the bottom liquid layer ($i = 2$), u_{L_i} and w_{L_i} are, respectively, the r and z components of the particle velocity.

Using Eqs. 7, 8, 11, and 12 in Eqs. 1–4 and 9, we obtain

$$\left(\nabla^2 - \frac{\partial^2}{\partial t^2}\right)\varphi + p_0\varphi^* - \left(T + \tau_1\frac{\partial T}{\partial t}\right) = 0, \tag{13}$$

$$\left(\nabla^2\psi - \frac{\psi}{r^2}\right) - \frac{p\varphi_\theta}{\delta^2} - \frac{1}{\delta^2}\frac{\partial^2\psi}{\partial t^2} = 0, \tag{14}$$

$$\left(\nabla^2 - \frac{1}{r^2}\right)\varphi_\theta + \delta^{*^2}\left(\nabla^2 - \frac{1}{r^2}\right)\psi - 2\delta^{*^2}\varphi_\theta - \frac{1}{\delta_1^2}\frac{\partial^2\varphi_\theta}{\partial t^2} = 0, \tag{15}$$

$$\nabla^2\varphi^* - p_1\delta_1^*\varphi^* - p_0\delta_1^*\nabla^2\varphi + \bar{\nu}\delta_1^*\left(T + \tau_1\frac{\partial T}{\partial t}\right) - \frac{1}{\delta_2^2}\frac{\partial^2\varphi^*}{\partial t^2} = 0, \tag{16}$$

$$\nabla^2 T - (\dot{T} + \tau_0\ddot{T}) = \in\left(\frac{\partial}{\partial t} + \eta_0\tau_0\frac{\partial^2}{\partial t^2}\right)\nabla^2\dot{\varphi} + \bar{\nu} \in \left(\frac{\partial}{\partial t} + \eta_0\tau_0\frac{\partial^2}{\partial t^2}\right)\varphi^*, \tag{17}$$

$$\nabla^2\varphi_{L_i} - \frac{1}{\delta_L^2}\frac{\partial^2\varphi_{L_i}}{\partial t^2} = 0 \quad i = 1, 2, \tag{18}$$

where

$$\nabla^2 = \frac{\partial^2}{\partial r^2} + \frac{1}{r}\frac{\partial}{\partial r} + \frac{\partial^2}{\partial z^2}.$$

3.1 Boundary Conditions

The boundary conditions at the solid–liquid interfaces $z = \pm d$ to be satisfied are as follows:

(i) The magnitude of the normal component of the stress tensor of the plate should be equal to the pressure of the liquid. $(t_{zz})_{\mathrm{S}} = (t_{zz})_{\mathrm{L}}$, implying that

$$\frac{\partial^2\varphi}{\partial t^2} - (2\delta^2 - p)\left(\frac{\partial^2\varphi}{\partial r^2} + \frac{1}{r}\frac{\partial\varphi}{\partial r} + \frac{\partial^2\psi}{\partial r\partial z}\right) = \omega^2\frac{\rho_{\mathrm{L}}}{\rho}\varphi_{\mathrm{L}_i}, \quad i = 1, 2. \tag{19}$$

(ii) The tangential component of the stress tensor should be zero.

$$(t_{zr})_{\mathrm{S}} = 0, \text{ implying that } \frac{\partial^2\psi}{\partial t^2} - (2\delta^2 - p) \times \left(\frac{\partial^2\psi}{\partial r^2} + \frac{1}{r}\frac{\partial\psi}{\partial r} - \frac{\psi}{r^2} - \frac{\partial^2\varphi}{\partial r\partial z}\right) = 0 \tag{20}$$

(iii) The tangential component of the couple stress tensor should be zero.

$$(m_{z\theta})_{\mathrm{S}} = 0, \text{ implying that } \frac{\partial \varphi_\theta}{\partial z} = 0 \tag{21}$$

(iv) The component of microstress tensor vanishes,

$$\lambda_z^* = 0 \tag{22}$$

(v) The normal velocity component of the solid should be equal to that of the liquid. $(\dot{u}_z)_{\mathrm{S}} = (\dot{w})_{\mathrm{L}}$

$$\text{This leads to } \frac{\partial}{\partial t}\left(\frac{\partial \varphi}{\partial z} - \frac{\partial \psi}{\partial r} - \frac{\psi}{r}\right) = \frac{\partial}{\partial t}\left(\frac{\partial \varphi_{\mathrm{L}_i}}{\partial z}\right), \quad i = 1, 2. \tag{23}$$

(vi) The thermal boundary condition is given by

$$T_{,z} + HT = 0 \tag{24}$$

where H is the surface heat transfer coefficient. Here, $H \to 0$ corresponds to thermally insulated boundaries and $H \to \infty$ refers to the isothermal one.

4 Formal Solution of the Problem

We assume solutions of Eqs. 13–18 of the form,

$$\begin{aligned}(\varphi, \psi, \varphi_\theta, T, \varphi^*, \varphi_{\mathrm{L}_1}, \varphi_{\mathrm{L}_2}) = [&f(z)J_0(\xi r), g(z)J_1(\xi r), w(z)J_1(\xi r), h(z)J_0(\xi r),\\ &\eta(z)J_0(\xi r), \bar{\varphi}_{\mathrm{L}_1}(z)J_0(\xi r), \bar{\varphi}_{\mathrm{L}_2}(z)J_0(\xi r)\big]\,\mathrm{e}^{-\mathrm{i}\omega t},\end{aligned} \tag{25}$$

where $c = \omega/\xi$ is the phase velocity, ω is the circular frequency, ξ is the wave number, and $J_0(\xi r)$ and $J_1(\xi r)$ are Bessel functions of order zero and one, respectively.

Using Eq. 25 in Eqs. 13–18 and solving the resulting differential equations, the expressions for φ, ψ, φ_θ, T, φ^*, φ_{L_1}, and φ_{L_2} are obtained as

$$\begin{aligned}\varphi = &(A_1 \cos m_1 z + A_2 \cos m_2 z + A_3 \cos m_3 z + B_1 \sin m_1 z + B_2 \sin m_2 z\\ &+ B_3 \sin m_3 z)J_0(\xi r)\mathrm{e}^{-\mathrm{i}\omega t},\end{aligned} \tag{26}$$

$$\psi = (A_4 \cos m_4 z + B_4 \sin m_4 z + A_5 \cos m_5 z + B_5 \sin m_5 z)J_1(\xi r)\mathrm{e}^{-\mathrm{i}\omega t}, \tag{27}$$

$$\begin{aligned}\varphi_\theta = &\frac{\delta^2}{p}[(b^2 - m_4^2)(A_4 \cos m_4 z + B_4 \sin m_4 z) + (b^2 - m_5^2)(A_5 \cos m_5 z\\ &+ B_5 \sin m_5 z)J_1(\xi r)\mathrm{e}^{-\mathrm{i}\omega t},\end{aligned} \tag{28}$$

$$\begin{aligned}T = &[S_1(A_1 \cos m_1 z + B_1 \sin m_1 z) + S_2(A_2 \cos m_2 z + B_2 \sin m_2 z)\\ &+ S_3(A_3 \cos m_3 z + B_3 \sin m_3 z)]J_0(\xi r)\mathrm{e}^{-\mathrm{i}\omega t},\end{aligned} \tag{29}$$

$$\varphi^* = [V_1(A_1\cos m_1 z + B_1\sin m_1 z) + V_2(A_2\cos m_2 z + B_2\sin m_2 z) + V_3(A_3\cos m_3 z + B_3\sin m_3 z)]J_0(\xi r)\mathrm{e}^{-\mathrm{i}\omega t}, \tag{30}$$

$$\varphi_{\mathrm{L}_1} = A_4\sin\gamma_{\mathrm{L}}[z-(d+h)]\,J_0(\xi r)\mathrm{e}^{-\mathrm{i}\omega t}, \quad d<z<d+h, \tag{31}$$

$$\varphi_{\mathrm{L}_2} = A_5\sin\gamma_{\mathrm{L}}[z+(d+h)]\,J_0(\xi r)\mathrm{e}^{-\mathrm{i}\omega t}, \quad -(d+h)<z<-d, \tag{32}$$

where

$$m_i^2 = \xi^2(c^2a_i^2-1),\ i=1,2,3,4,5; \quad a^2=\xi^2(c^2-1),$$

$$b^2 = \xi^2\left(\frac{c^2}{\delta^2}-1\right), \quad \gamma_{\mathrm{L}}^2 = \xi^2\left(\frac{c^2}{\delta_{\mathrm{L}}^2}-1\right)$$

$$\sum a_i^2 = 1+k_0+\frac{1}{\delta_2^2}-\frac{p_1\delta_1^*}{\omega^2}+\frac{p_0^2\delta_1^*}{\omega^2}-i\omega\in k_1k_0',$$

$$\sum a_i^2a_j^2 = k_0+\frac{1+k_0}{\delta_2^2}-\frac{\delta_1^*}{\omega^2}\Big[(1+k_0)p_1-p_0^2k_0+i\omega\in k_0'k_1(\bar{\nu}p_0-p_1) -i\omega\in k_0'k_1\bar{\nu}(\bar{\nu}-p_0)\Big]-\frac{i\omega\in k_0'k_1}{\delta_2^2},$$

$$a_1^2a_2^2a_3^2 = k_0\left(\frac{1}{\delta_2^2}-\frac{p_1\delta_1^*}{\omega^2}\right)-\frac{ik_0'k_1\in\delta_1^*\bar{\nu}^2}{\omega}, \quad a_4^2+a_5^2=\frac{1}{\delta^2}+\frac{1}{\delta_1^2} +\frac{\delta^*\left(p-2\delta^2\right)}{\omega^2\delta^2}, \quad a_4^2a_5^2=\frac{1}{\delta^2}\left(\frac{1}{\delta_1^2}-\frac{2\delta^*}{\omega^2}\right)$$

$$k_0=\tau_0+i\omega^{-1}, \quad k_0'=\eta_0\tau_0+i\omega^{-1}, \quad k_1=\tau_1+i\omega^{-1},$$

$$V_i = \frac{-\delta_1^*\left[(\bar{\nu}-p_0)m_i^2-\bar{\nu}\xi^2\left(c^2+\frac{p_0}{\bar{\nu}}-1\right)\right]}{m_i^2-\xi^2\left[c^2\left(\frac{1}{\delta_2^2}-\frac{\delta_1^*}{\omega^2}(\bar{\nu}p_0-p_1)\right)-1\right]}, \quad i,j=1,2,3$$

$$S_i = \frac{\left[m_i^2-\xi^2(c^2-1)\right]\left[m_i^2-\xi^2\left(c^2\left(\frac{1}{\delta_2^2}-\frac{\delta_1^*}{\omega^2}(\bar{\nu}p_0-p_1)\right)-1\right)\right] +\delta_1^*p_0\left[(\bar{\nu}-p_0)m_i^2-\bar{\nu}\xi^2\left(c^2+\frac{p_0}{\bar{\nu}}-1\right)\right]}{i\omega k_1\left[m_i^2-\xi^2\left(c^2\left(\frac{1}{\delta_2^2}-\frac{\delta_1^*}{\omega^2}(\bar{\nu}p_0-p_1)\right)-1\right)\right]}$$

The main difference between this case and leaky Lamb waves is that the functions φ_{L_1} and φ_{L_2} here are chosen in such a way that the acoustical pressure is zero at $z=\pm(d+h)$; in other words, φ_{L_1} and φ_{L_2} here are of standing wave solutions, for leaky Lamb waves, they are traveling waves.

5 Derivation of the Secular Equations

Using the boundary conditions, Eqs. 19–24 on the surfaces $z = \pm d$ of the plate and using Eqs. 26–32, we obtain a system of 12 simultaneous equations which has a non-trivial solution if the determinant of the coefficients of amplitudes $[A_1, A_2, A_3, A_4, A_5, B_1, B_2, B_3, B_4, B_5, A_6, A_7]^{\mathrm{T}}$ vanishes.

We obtain the following secular equations after applying lengthy algebraic reductions and manipulations along with the conditions $\gamma_{\mathrm{L}} \neq 0$ and $\gamma_{\mathrm{L}} \neq (2n-1)\frac{\pi}{2}$, $n = 1, 2, 3, \ldots,$

$$
\begin{aligned}
&\left[\frac{T_1}{T_4}\right]^{\pm 1} - \frac{m_1(V_1S_3 - V_3S_1)}{m_2(V_2S_3 - V_3S_2)}\left[\frac{T_2}{T_4}\right]^{\pm 1} + \frac{m_1(V_1S_2 - V_2S_1)}{m_3(V_2S_3 - V_3S_2)}\left[\frac{T_3}{T_4}\right]^{\pm 1} \\
&\quad + \frac{RV}{SU}\frac{(f_5 - f_4)}{(m_5 f_5 T_4 - m_4 f_4 T_5)}\frac{m_1 S_1(V_3 - V_2)}{m_2 m_3(V_2S_3 - V_3S_2)}\left\{\left[\frac{T_2T_3}{T_4^2T_5}\right]^{\pm 1}\right. \\
&\quad \left. - \frac{m_2S_2(V_3 - V_1)}{m_1S_1(V_3 - V_2)}\left[\frac{T_1T_3}{T_4^2T_5}\right]^{\pm 1} + \frac{m_3S_3(V_2 - V_1)}{m_1S_1(V_3 - V_2)}\left[\frac{T_1T_2}{T_4^2T_5}\right]^{\pm 1}\right\} \\
&\quad + \frac{Q}{P}\frac{[m_4 - m_5(\frac{T_5}{T_4})^{\pm 1}]}{[m_5 f_5 - m_4 f_4(\frac{T_5}{T_4})^{\pm 1}]} \\
&\quad \times \left\{\begin{array}{l} \frac{V}{U}\frac{f_5 f_4(S_3 - S_2)}{(V_2S_3 - V_3S_2)}\left[\left[\frac{T_1}{T_4}\right]^{\pm 1} - \frac{m_1(S_3 - S_1)}{m_2(S_3 - S_2)}\left[\frac{T_2}{T_4}\right]^{\pm 1} + \frac{m_1(S_2 - S_1)}{m_3(S_3 - S_2)}\left[\frac{T_3}{T_4}\right]^{\pm 1}\right] \\ \quad + \frac{R}{S}\left[\left[\frac{T_1}{T_4}\right]^{\pm 1} - \frac{m_1V_2(V_1S_3 - V_3S_1)}{m_2V_1(V_2S_3 - V_3S_2)}\left[\frac{T_2}{T_4}\right]^{\pm 1} + \frac{m_1V_3(V_1S_2 - V_2S_1)}{m_3V_1(V_2S_3 - V_3S_2)}\left[\frac{T_3}{T_4}\right]^{\pm 1}\right] \end{array}\right\} \\
&\quad + \frac{\rho_{\mathrm{L}}\omega^2 T_6}{\rho\delta^2\gamma_{\mathrm{L}}}\frac{(\frac{1}{P} + \frac{i\xi Q}{P^2})}{(V_2S_3 - V_3S_2)} \\
&\quad \times \left\{\begin{array}{l} S_1m_1(V_3 - V_2)\left[1 + \frac{S_3(V_2 - V_1)}{S_1(V_3 - V_2)} - \frac{S_2(V_3 - V_1)}{S_1(V_3 - V_2)}\right]\left[\frac{1}{T_4}\right]^{\pm 1} + \frac{RV}{SU}\frac{(f_5 - f_4)V_1(S_3 - S_2)}{(m_5 f_5 T_4 - m_4 f_4 T_5)} \\ \times \left[\left[\frac{T_1}{T_4^2T_5}\right]^{\pm 1} - \frac{m_1V_2(S_3 - S_1)}{m_2V_1(S_3 - S_2)}\left[\frac{T_2}{T_4^2T_5}\right]^{\pm 1} + \frac{m_1V_3(S_2 - S_1)}{m_3V_1(S_3 - S_2)}\left[\frac{T_3}{T_4^2T_5}\right]^{\pm 1}\right] \end{array}\right\} \\
&= \frac{-Q^2m_1m_4m_5((V_1 - V_2)(S_2 - S_3) - (V_2 - V_3)(S_1 - S_2))(f_5 - f_4)}{P^2(V_2S_3 - V_3S_2)[m_5f_5 - m_4f_4(\frac{T_5}{T_4})^{\pm 1}]} \\
&\quad - \frac{Q^2}{P^2}\frac{RV}{SU}\frac{(m_5f_4T_4 - m_4f_5T_5)}{(m_5f_5T_4 - m_4f_4T_5)}\frac{V_1(S_3 - S_2)}{(V_2S_3 - V_3S_2)} \\
&\quad \times \left\{\left[\frac{T_1}{T_4}\right]^{\pm 1} - \frac{m_1V_2(S_3 - S_1)}{m_2V_1(S_3 - S_2)}\left[\frac{T_2}{T_4}\right]^{\pm 1} + \frac{m_1V_3(S_2 - S_1)}{m_3V_1(S_3 - S_2)}\left[\frac{T_3}{T_4}\right]^{\pm 1}\right\} \qquad (33)
\end{aligned}
$$

for stress-free thermally insulated boundaries ($H \to 0$) of the plate.

$$
\left[\frac{T_1}{T_4}\right]^{\pm 1} - \frac{m_1S_2(V_3 - V_1)}{m_2S_1(V_3 - V_2)}\left[\frac{T_2}{T_4}\right]^{\pm 1} + \frac{m_1S_3(V_2 - V_1)}{m_3S_1(V_3 - V_2)}\left[\frac{T_3}{T_4}\right]^{\pm 1}
$$

$$
\begin{aligned}
&+\frac{RV}{SU}\frac{(m_5f_4T_4-m_4f_5T_5)}{m_4m_5(f_5-f_4)}\frac{m_1(V_2S_3-V_3S_2)}{m_2m_3S_1(V_3-V_2)}\left\{\left[\frac{T_2T_3}{T_4}\right]^{\pm1}\right.\\
&\left.-\frac{m_2(V_1S_3-V_3S_1)}{m_1(V_2S_3-V_3S_2)}\left[\frac{T_1T_3}{T_4}\right]^{\pm1}+\frac{m_3(V_1S_2-V_2S_1)}{m_1(V_2S_3-V_3S_2)}\left[\frac{T_1T_2}{T_4}\right]^{\pm1}\right\}\\
&+\frac{P}{Q}\frac{(m_4T_5-m_5T_4)}{m_4m_5(f_5-f_4)}\\
&\times\left\{\begin{array}{l}\frac{U}{V}\frac{m_1f_5f_4(S_3-S_2)}{m_2m_3S_1(V_3-V_2)}\left[\left[\frac{T_2T_3}{T_4}\right]^{\pm1}-\frac{m_2(S_3-S_1)}{m_1(S_3-S_2)}\left[\frac{T_1T_3}{T_4}\right]^{\pm1}+\frac{m_3(S_2-S_1)}{m_1(S_3-S_2)}\left[\frac{T_1T_2}{T_4}\right]^{\pm1}\right]\\
\quad+\frac{R}{S}\frac{m_1V_1(V_2S_3-V_3S_2)}{m_2m_3S_1(V_3-V_2)}\left[\begin{array}{l}\left[\frac{T_2T_3}{T_4}\right]^{\pm1}-\frac{m_2V_2(V_1S_3-V_3S_1)}{m_1V_1(V_2S_3-V_3S_2)}\left[\frac{T_1T_3}{T_4}\right]^{\pm1}\\ \quad+\frac{m_3V_3(V_1S_2-V_2S_1)}{m_1V_1(V_2S_3-V_3S_2)}\left[\frac{T_1T_2}{T_4}\right]^{\pm1}\end{array}\right]\end{array}\right\}\\
&+\frac{\rho_L\omega^2T_6}{\rho\delta^2\gamma_Lm_4m_5}\frac{\left(\frac{P}{Q^2}+\frac{i\xi}{Q}\right)}{(V_2S_3-V_3S_2)}\\
&\times\left\{\begin{array}{l}\frac{(m_5f_5T_4-m_4f_4T_5)}{(f_5-f_4)}\left[\left[\frac{T_1}{T_4}\right]^{\pm1}-\frac{m_1S_2(V_3-V_1)}{m_2S_1(V_3-V_2)}\left[\frac{T_2}{T_4}\right]^{\pm1}+\frac{m_1S_3(V_2-V_1)}{m_3S_1(V_3-V_2)}\left[\frac{T_3}{T_4}\right]^{\pm1}\right]\\
\quad+\frac{RV}{SU}\frac{m_1(V_2S_3-V_3S_2)}{m_2m_3S_1(V_3-V_2)}\left[\begin{array}{l}\left[\frac{T_2T_3}{T_4^2T_5}\right]^{\pm1}-\frac{m_2(V_1S_3-V_3S_1)}{m_1(V_2S_3-V_3S_2)}\left[\frac{T_1T_3}{T_4^2T_5}\right]^{\pm1}\\ \quad+\frac{m_3(V_1S_2-V_2S_1)}{m_1(V_2S_3-V_3S_2)}\left[\frac{T_1T_2}{T_4^2T_5}\right]^{\pm1}\end{array}\right]\end{array}\right\}\\
&=\frac{V_2(S_3-S_1)\left[1-\frac{m_4f_4}{m_5f_5}(\frac{T_5}{T_4})^{\pm1}\right]f_5P^2}{Q^2m_3m_4S_1(V_3-V_2)(f_5-f_4)}\left\{\left[\frac{T_1T_3}{T_4^2}\right]^{\pm1}\right.\\
&\left.-\frac{m_1V_1(S_3-S_2)}{m_2V_2(S_3-S_1)}\left[\frac{T_2T_3}{T_4^2}\right]^{\pm1}-\frac{m_3V_3(S_2-S_1)}{m_2V_2(S_3-S_1)}\left[\frac{T_1T_2}{T_4^2}\right]^{\pm1}\right\}\\
&+\frac{P^2}{Q^2}\frac{RV}{SU}\frac{S_2(V_3-V_1)}{S_1(V_3-V_2)m_2m_3m_4m_5}\left[\frac{T_1T_2T_3}{T_4^2T_5}\right]^{\pm1}\\
&\times\left\{1-\frac{S_1(V_3-V_2)}{S_2(V_3-V_1)}-\frac{S_3(V_2-V_1)}{S_2(V_3-V_1)}\right\}
\end{aligned}
\tag{34}
$$

for stress-free isothermal boundaries ($H\to\infty$) of the plate, where

$$
\begin{aligned}
&P=b^2-\xi^2+\frac{p\xi^2}{\delta^2},\quad Q=-2\xi\left(1-\frac{p}{2\delta^2}\right),\quad f_i=b^2-m_i^2,\quad i=4,5;\\
&R=i\xi b_0,\quad S=\frac{\gamma\delta^2}{p},\quad U=\alpha_0,\quad V=\frac{b_0i\xi\delta^2}{p},\\
&T_i=\tan m_id,\quad i=1,2,3,4,5;\quad T_6=\tan\gamma_Lh.
\end{aligned}
$$

Here the superscript +1 refers to skew-symmetric and −1 refers to symmetric modes. Equations 33 and 34 are the most general dispersion relations involving the wave number and phase velocity of various modes of propagation in thermo-microstretch elastic plates bordered with layers of inviscid liquid on both sides. These equations can be recognized as modified Rayleigh–Lamb equations which, respectively, govern the symmetric and antisymmetric modes of wave propagation for stress and couple stress-free, thermally insulated and isothermal thermo-microstretch elastic plate. We refer to such waves as thermo-microstretch elastic plate waves rather than Lamb waves whose properties were derived by Lamb [14] for isotropic elastic solids in elastokinetics. Thus, Rayleigh–Lamb type equation also governs circular-crested thermo-microstretch elastic waves in a plate. Although the frequency wave number relationship holds whether the waves are straight or circularly crested, the displacement, microrotation, temperature, microstretch, and stresses vary according to Bessel functions rather than trigonometric functions as far as the radial coordinate is concerned. For large value of r, we have

$$J_0(\xi r) \to \frac{\sin \xi r + \cos \xi r}{\sqrt{\pi \xi r}}, \quad J_1(\xi r) \to \frac{\sin \xi r - \cos \xi r}{\sqrt{\pi \xi r}}.$$

Thus, far from the origin, the motion becomes periodic in r. Actually, "far" occurs rather rapidly, within four to five zeros of the Bessel function. As r becomes very large, the straight crested behavior is the limit of the circular-crested waves.

If we let ρ_{L} approach zero, Eqs. 33 and 34 recover the dispersion equations for Lamb-type waves of free boundaries in a thermo-microstretch elastic plate.

5.1 Particular Cases

(a) Thermo-microstretch elastic plate with one relaxation time [Lord and Shulman (L-S) theory]
In this case, $\tau_1 = 0$, $\tau_0 > 0$, and $\eta_0 = 1$.
(b) Thermo-microstretch elastic plate with two relaxation times (G-L theory)
In this case, $\tau_1 \geq \tau_0 > 0$, and $\eta_0 = 0$.
(c) Micropolar thermoelastic plate
In this case, $\alpha_0 = \lambda_1 = b_0 = \lambda_0 = 0$.

6 Regions of the Secular Equation

To explore various regions of the secular equations, we consider Eq. 33 as an example for the purpose of discussion. Depending upon whether $m_1, m_2, m_3, m_4, m_5, b$, and γ_L are real, purely imaginary, or complex, the frequency equations, Eqs. 33 and 34, are correspondingly altered as follows.

6.1 Region I

When the characteristic roots are of the type, $a^2 = -a'^2$, $\beta^2 = -\beta'^2$, $m_k^2 = -\alpha_k^2$, $k = 1, 2, 3, 4, 5$ so that $a = \mathrm{i}\,a'$, $b = \mathrm{i}\,b'$, $\gamma_\mathrm{L} = \mathrm{i}\gamma'_\mathrm{L}$, and $m_k = \mathrm{i}\,\alpha_k$, $k = 1, 2, 3, 4, 5$ are purely imaginary or complex numbers. This ensures that the superposition of partial waves has the property of exponential decay. In this case, the secular equations are written from Eqs. 33 and 34 by replacing circular tangent functions of $m_k, \gamma_\mathrm{L}; k = 1, 2, 3, 4, 5$ with hyperbolic tangent functions of $\alpha_k, \gamma'_\mathrm{L}; k = 1, 2, 3, 4, 5$.

6.2 Region II

This region is characterized by $\delta < c < 1$. In this case, we have $b = b$, $\gamma_\mathrm{L} = \gamma_\mathrm{L}$, $m_4 = m_4$, $m_5 = m_5$, $a = \mathrm{i}\,a'$, $m_k = \mathrm{i}\,\alpha_k$, $(k = 1, 2, 3)$ and the secular equations can be obtained from Eqs. 33 and 34 by replacing circular tangent functions of m_k, $k = 1, 2, 3$ with hyperbolic tangent functions of α_k, $k = 1, 2, 3$.

6.3 Region III

In this case, the characteristic roots are given by m_k^2, $k = 1, 2, 3, 4, 5$ and the secular equation is given by Eqs. 33 and 34.

7 Waves of Short Wavelength

Some information on the asymptotic behavior is obtained by letting $\xi \to \infty$; $\frac{\tanh \alpha_i d}{\tanh \alpha_j d} \to 1$, $\frac{\tanh \gamma_\mathrm{L} h}{\tanh \alpha_j d} \to 1$, $i = 1, 2, 3$, $j = 4, 5$. If we take $\xi > \frac{\omega}{\delta}$, it follows that $c < \delta, 1$. In this case, the roots of the secular equation lie in Region I and we replace a, b, γ_L, and m_k with $\mathrm{i}\,a'$, ib', $\mathrm{i}\gamma'_\mathrm{L}$, and $\mathrm{i}\alpha_k$, $k = 1, 2, 3, 4, 5$, respectively, so that secular equations 33 and 34 reduce to

$$
\begin{aligned}
&\left(b'^2 - \alpha_4^2 - \alpha_5^2 - \alpha_4\alpha_5\right)\left[\alpha_2\alpha_3(V'_2S'_3 - V'_3S'_2) - \alpha_1\alpha_3(V'_1S'_3 - V'_3S'_1)\right.\\
&\left.+\alpha_1\alpha_2(V'_1S'_2 - V'_2S'_1)\right]\\
&+\frac{RV}{SU}(\alpha_4 + \alpha_5)\left[\alpha_1 S'_1(V'_3 - V'_2) - \alpha_2 S'_2(V'_3 - V'_1) + \alpha_3 S'_3(V'_2 - V'_1)\right]\\
&+\frac{QV}{PU}\left\{\alpha_4^2\alpha_5^2 - b'^2(\alpha_4^2 + \alpha_5^2 - b'^2)\right\}\left[\alpha_3\alpha_2(S'_3 - S'_2) - \alpha_1\alpha_3(S'_3 - S'_1)\right.\\
&\left.+\alpha_1\alpha_2(S'_2 - S'_1)\right]\\
&+\frac{QR}{PS}\left[\alpha_2\alpha_3 V'_1(V'_2S'_3 - V'_3S'_2) - \alpha_1\alpha_3 V'_2(V'_1S'_3 - V'_3S'_1)\right.\\
&\left.+\alpha_1\alpha_2 V'_3(V'_1S'_2 - V'_2S'_1)\right]\\
&+\frac{\rho_L\omega^2}{\rho\delta^2\gamma'_\mathrm{L}}\left(\frac{1}{P} + \frac{i\xi Q}{P^2}\right)\left[\alpha_1\alpha_2\alpha_3\left[(V'_1 - V'_2)(S'_2 - S'_3) - (V'_2 - V'_3)(S'_1 - S'_2)\right]\right.
\end{aligned}
$$

$$+\frac{RV}{SU}(\alpha_4+\alpha_5)\left[\alpha_3\alpha_2V_1'(S_3'-S_2')-\alpha_1\alpha_3V_2'(S_3'-S_1')+\alpha_1\alpha_2V_3'(S_2'-S_1')\right]\Bigg]$$

$$=-\frac{Q^2(\alpha_4\alpha_5-b'^2)}{P^2}\frac{RV}{SU}\left[\alpha_3\alpha_2V_1'(S_3'-S_2')-\alpha_1\alpha_3V_2'(S_3'-S_1')\right.$$

$$\left.+\alpha_1\alpha_2V_3'(S_2'-S_1')\right]$$

$$-\frac{Q^2}{P^2}\alpha_1\alpha_2\alpha_3\alpha_4\alpha_5(\alpha_4+\alpha_5)\left[(V_1'-V_2')(S_2'-S_3')-(V_2'-V_3')(S_1'-S_2')\right] \quad (35)$$

$$\left[\alpha_2\alpha_3S_1'(V_3'-V_2')-\alpha_1\alpha_3S_2'(V_3'-V_1')+\alpha_1\alpha_2S_3'(V_2'-V_1')\right]$$

$$+\frac{RV}{SU}\frac{(b^2-\alpha_4\alpha_5)}{\alpha_4\alpha_5(\alpha_4+\alpha_5)}\left[\alpha_1(V_2'S_3'-V_3'S_2')-\alpha_2(V_1'S_3'-V_3'S_1')\right.$$

$$\left.+\alpha_3(V_1'S_2'-V_2'S_1')\right]$$

$$+\frac{PU}{QV}\frac{\left\{\alpha_4^2\alpha_5^2-b'^2\left(\alpha_4^2+\alpha_5^2-b'^2\right)\right\}}{\alpha_4\alpha_5(\alpha_4+\alpha_5)}\left[\alpha_1(S_3'-S_2')-\alpha_2(S_3'-S_1')\right.$$

$$\left.+\alpha_3(S_2'-S_1')\right]$$

$$+\frac{\rho_L\omega^2}{\rho\delta^2\gamma_L'\alpha_4\alpha_5}\left(\frac{P}{Q^2}+\frac{i\xi}{Q}\right)$$

$$\times\left\{\begin{array}{l}\frac{(\alpha_4^2+\alpha_5^2+\alpha_4\alpha_5-b'^2)}{(\alpha_4+\alpha_5)}\left[\alpha_2\alpha_3S_1'(V_3'-V_2')-\alpha_1\alpha_3S_2'(V_3'-V_1')\right.\\ \left.+\alpha_1\alpha_2S_3'(V_2'-V_1')\right]\\ +\frac{RV}{SU}\left[\alpha_1(V_2'S_3'-V_3'S_2')-\alpha_2(V_1'S_3'-V_3'S_1')+\alpha_3(V_1'S_2'-V_2'S_1')\right]\end{array}\right\}$$

$$+\frac{PR}{QS}\frac{\left\{\alpha_4^2\alpha_5^2-b'^2\left(\alpha_4^2+\alpha_5^2-b'^2\right)\right\}}{\alpha_4\alpha_5(\alpha_4+\alpha_5)}\left[\alpha_1V_1'(V_2'S_3'-V_3'S_2')\right.$$

$$\left.-\alpha_2V_2'(V_1'S_3'-V_3'S_1')+\alpha_3V_3'(V_1'S_2'-V_2'S_1')\right]$$

$$=\left[\alpha_2V_2'(S_3'-S_1')-\alpha_3V_3'(S_2'-S_1')-\alpha_1V_1'(S_3'-S_2')\right]$$

$$\times\frac{P^2(b'^2-\alpha_4^2-\alpha_5^2-\alpha_4\alpha_5)}{Q^2\alpha_4\alpha_5(\alpha_4+\alpha_5)}$$

$$+\frac{P^2}{Q^2\alpha_4\alpha_5}\frac{RV}{SU}[V_1'(S_3'-S_2')-V_2'(S_3'-S_1')+V_3'(S_2'-S_1')]. \quad (36)$$

Equations 35 and 36 are, respectively, the Rayleigh surface wave equations for a stress and couple stress free thermally insulated and isothermal, thermo-microstretch elastic half-space bordered with inviscid liquid layers.

8 Amplitudes of Dilatation, Microrotation, Microstretch, and Temperature

In this section, the amplitudes of dilatation, microrotation, microstretch, and temperature distribution for symmetric and skew-symmetric modes of plate waves have been computed for a stress-free thermo-microstretch elastic plate. Upon using Eqs. 11 and 26–30, we obtain

$$
\begin{aligned}
(e)_{\mathrm{sym}} &= -\Big\{(\xi^2+m_1^2)\cos m_1 z + L(\xi^2+m_2^2)\cos m_2 z \\
&\quad + M(\xi^2+m_3^2)\cos m_3 z\Big\} A_1 J_0(\xi r)\mathrm{e}^{-\mathrm{i}\omega t}, \\
(e)_{\mathrm{asym}} &= \Big\{(\xi^2+m_1^2)\sin m_1 z + L'(\xi^2+m_2^2)\sin m_2 z \\
&\quad + M'(\xi^2+m_3^2)\sin m_3 z\Big\} B_1 J_0(\xi r)\mathrm{e}^{-\mathrm{i}\omega t}, \\
(\varphi_\theta)_{\mathrm{sym}} &= \frac{\delta^2}{p}\left\{(b^2-m_4^2)\cos m_4 z - (b^2-m_5^2)\frac{f_4 m_4 s_4}{f_5 m_5 s_5}\cos m_5 z\right\} A_4 J_1(\xi r)\mathrm{e}^{-\mathrm{i}\omega t}, \\
(\varphi_\theta)_{\mathrm{asym}} &= \frac{\delta^2}{p}\left\{(b^2-m_4^2)\sin m_4 z - (b^2-m_5^2)\frac{f_4 m_4 C_4}{f_5 m_5 C_5}\sin m_5 z\right\} B_4 J_1(\xi r)\mathrm{e}^{-\mathrm{i}\omega t}, \\
(\varphi^*)_{\mathrm{sym}} &= \{V_1\cos m_1 z + V_2 L\cos m_2 z + V_3 M\cos m_3 z\} A_1 J_0(\xi r)\mathrm{e}^{-\mathrm{i}\omega t}, \\
(\varphi^*)_{\mathrm{asym}} &= \{V_1\sin m_1 z + V_2 L'\sin m_2 z + V_3 M'\sin m_3 z\} B_1 J_0(\xi r)\mathrm{e}^{-\mathrm{i}\omega t} \\
(T)_{\mathrm{sym}} &= \{S_1\cos m_1 z + S_2 L\cos m_2 z + S_3 M\cos m_3 z\} A_1 J_0(\xi r)\mathrm{e}^{-\mathrm{i}\omega t}, \\
(T)_{\mathrm{asym}} &= \{S_1\sin m_1 z + S_2 L'\sin m_2 z + S_3 M'\sin m_3 z\} B_1 J_0(\xi r)\mathrm{e}^{-\mathrm{i}\omega t},
\end{aligned}
$$

where

$$
\begin{aligned}
L &= \frac{(V_3S_1 - V_1S_3)m_1 s_1}{(V_2S_3 - V_3S_2)m_2 s_2}, \quad L' = \frac{(V_3S_1 - V_1S_3)m_1 C_1}{(V_2S_3 - V_3S_2)m_2 C_2}, \\
M &= \frac{(V_1S_2 - V_2S_1)}{(V_2S_3 - V_3S_2)}\frac{m_1 s_1}{m_3 s_3}, \quad M' = \frac{(V_1S_2 - V_2S_1)}{(V_2S_3 - V_3S_2)}\frac{m_1 C_1}{m_3 C_3}, \\
s_i &= \sin m_i d,\ C_i = \cos m_i d, \quad i = 1,2,3,4,5.
\end{aligned}
$$

9 Numerical Results and Discussion

With the view of illustrating theoretical results obtained in the preceding sections and comparing these in the context of various theories of thermoelasticity, we now present some numerical results for magnesium crystal (thermo-microstretch elastic solid), the physical data for which is given below.

Micropolar parameters are

$$
\begin{aligned}
&\rho = 1.74\times10^3\,\mathrm{kg\cdot m^{-3}}, \quad \lambda = 9.4\times10^{10}\,\mathrm{N\cdot m^{-2}}, \quad \mu = 4.0\times10^{10}\,\mathrm{N\cdot m^{-2}}, \\
&K = 1.0\times10^{10}\,\mathrm{N\cdot m^{-2}}, \quad \gamma = 0.779\times10^{-9}\,\mathrm{N}, \quad j = 0.2\times10^{-19}\,\mathrm{m^2}, \\
&j_0 = 0.185\times10^{-19}\,\mathrm{m^2}
\end{aligned}
$$

Thermal parameters are

$$
\begin{aligned}
&\tau_0 = 6.131\times10^{-13}\,\mathrm{s}, \quad \tau_1 = 8.765\times10^{-13}\,\mathrm{s}, \quad \in = 0.028, \quad T_0 = 298\,\mathrm{K}, \\
&C^* = 1.04\times10^3\,\mathrm{J\cdot kg^{-1}\cdot K^{-1}}, \quad K^* = 1.7\times10^6\,\mathrm{J\cdot m^{-1}\cdot s^{-1}\cdot K^{-1}}, \\
&\nu = 2.68\times10^6\,\mathrm{N\cdot m^{-2}\cdot K^{-1}}, \quad \nu_1 = 2.0\times10^6\,\mathrm{N\cdot m^{-2}\cdot K^{-1}}
\end{aligned}
$$

and stretch parameters are

$$\lambda_0 = 0.5 \times 10^{10}\,\mathrm{N \cdot m^{-2}}, \quad \lambda_1 = 0.5 \times 10^{10}\,\mathrm{N \cdot m^{-2}}, \quad \alpha_0 = 0.779 \times 10^{-9}\,\mathrm{N},$$
$$b_0 = 0.5 \times 10^{-09}\,\mathrm{N}, \quad d = 0.01\,\mathrm{m}.$$

The liquid taken for the purpose of numerical calculations is water, and the speed of sound in water is given by $c_{\mathrm{L}} = 1.5 \times 10^3\,\mathrm{m \cdot s^{-1}}$.

A FORTRAN program has been developed for the solution of Eqs. 33 to compute the phase velocity c for different values of n by using the relations, $\tan\theta = \tan(n\pi + \theta)$ and $m_i^2 = \xi^2(c^2 a_i^2 - 1)$.

In general, the wave number and phase velocity of the waves are complex quantities; therefore, the waves are attenuated in space. If we write

$$c^{-1} = s^{-1} + \mathrm{i}\omega^{-1} q \tag{37}$$

then $\xi = K_1 + \mathrm{i}\, q$, where $K_1 = \omega/s$ and q are real numbers. This shows that s is the propagation speed and q is the attenuation coefficient of waves. Upon using Eq. 37 in the FORTRAN program developed for the solution of Eq. 33 to compute the phase velocity c, the attenuation coefficient q for different modes of wave propagation can be obtained.

The dimensionless phase velocity and attenuation coefficient of symmetric and skew-symmetric modes of wave propagation in the context of L-S and G-L theories of thermoelasticity have been computed for various values of a dimensionless wave number from dispersion Eq. 33, for a stress-free thermo-microstretch elastic plate bordered with layers of inviscid liquid on both sides and have been represented graphically for different modes ($n = 0$ to $n = 2$) in Figs. 1, 2, 3, and 4. The amplitudes of dilatation, microrotation, microstretch, and temperature distribution for symmetric and skew-symmetric modes in the context of L-S and G-L theories of thermoelasticity are presented graphically in Figs. 5, 6, 7, 8, 9, 10, 11, and 12. The broken lines correspond to the L-S theory, and solid curves correspond to the G-L theory of thermoelasticity.

9.1 Phase Velocity

The phase velocities of higher modes of propagation, symmetric, and skew-symmetric attain quite large values at a vanishing wave number which sharply slashes down to become steady and asymptotic to the reduced Rayleigh wave velocity with an increasing wave number.

It is observed from Fig. 1 that (i) for the lowest symmetric mode $n = 0$, the phase velocity for the G-L theory is quite less than in the case of the L-S theory for a wave number $\xi \leq 3.2$, the phase velocity for G-L theory is slightly more than in the case of the L-S theory for a wave number between 3.2 and 4.2, phase velocity profiles in respect of L-S and G-L theories coincide for wave number $\xi \geq 4.2$ and (ii) phase velocity profiles in respect of L-S and G-L theories coincide for first and second symmetric ($n = 1$ and $n = 2$) modes.

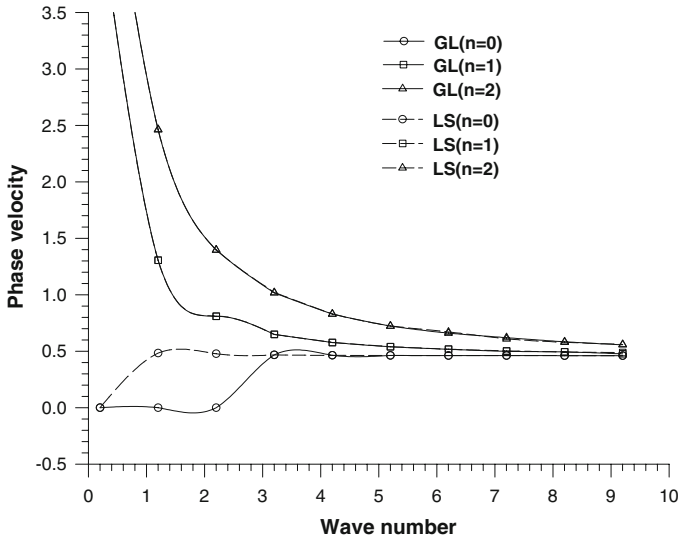

Fig. 1 Variation of phase velocity of symmetric modes of wave propagation (for L-S theory, $\tau_1 = 0$, $\tau_0 > 0$, and $\eta_0 = 1$, and for G-L theory, $\tau_1 \geq \tau_0 > 0$, and $\eta_0 = 0$)

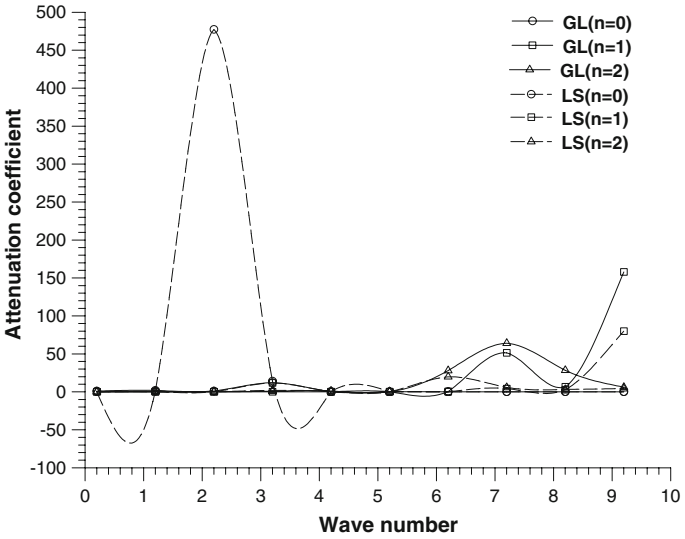

Fig. 2 Variation of attenuation coefficient of symmetric modes of wave propagation (for L-S theory, $\tau_1 = 0$, $\tau_0 > 0$, and $\eta_0 = 1$, and for G-L theory, $\tau_1 \geq \tau_0 > 0$, and $\eta_0 = 0$)

For skew-symmetric modes of wave propagation, we observe from Fig. 3 the following: (a) for $n = 0$, the phase velocity for the G-L theory is more than in the case of the L-S theory for wave number $\xi \leq 0.8$; the phase velocity for the G-L theory is less than in the case of the L-S theory for a wave number between 0.8 and 2.2; and the phase velocity profiles for L-S and G-L theories coincide for a wave number

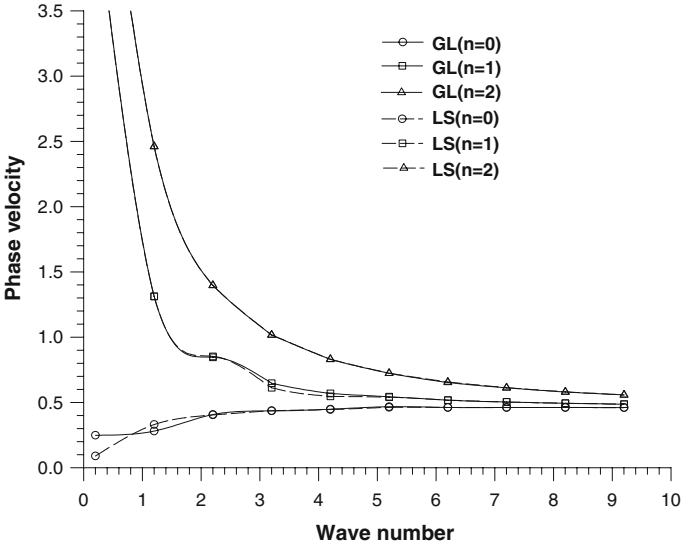

Fig. 3 Variation of phase velocity of skew-symmetric modes of wave propagation (for L-S theory, $\tau_1 = 0$, $\tau_0 > 0$, and $\eta_0 = 1$, and for G-L theory, $\tau_1 \geq \tau_0 > 0$, and $\eta_0 = 0$)

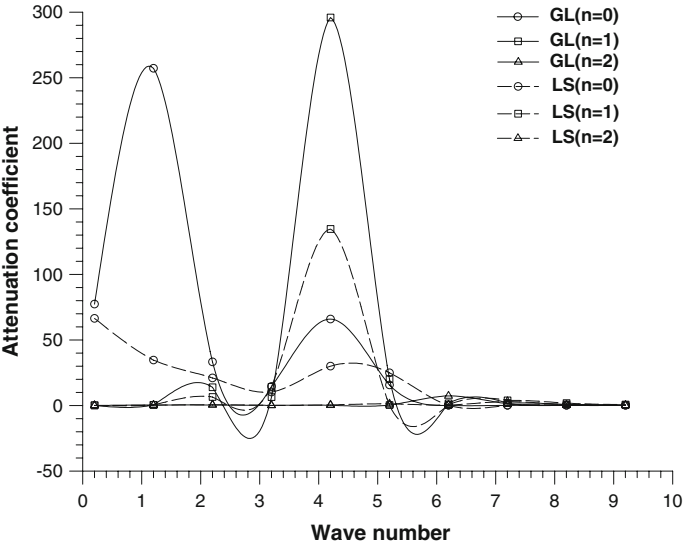

Fig. 4 Variation of attenuation coefficient of skew-symmetric modes of wave propagation (for L-S theory, $\tau_1 = 0$, $\tau_0 > 0$, and $\eta_0 = 1$, and for G-L theory, $\tau_1 \geq \tau_0 > 0$, and $\eta_0 = 0$)

$\xi \geq 2.2$, (b) for $n = 1$, the phase velocity profiles for L-S and G-L theories coincide for a wave number $\xi \leq 2.6$ and for a wave number between 5.0 and 9.2; and the phase velocity for the G-L theory is slightly more than in the case of the L-S theory for a

wave number between 2.6 and 5.0, and (c) for $n = 2$, the phase velocity profiles for L-S and G-L theories coincide.

9.2 Attenuation Coefficient

The variation of the attenuation coefficient with wave number for symmetric and skew-symmetric modes of a thermo-microstretch elastic plate bordered with layers of inviscid liquid on both sides is represented graphically in Figs. 2 and 4, respectively.

We observe the following from Fig. 2: (i) for the lowest symmetric mode, the magnitude of the attenuation coefficient for the G-L theory has negligible variation with wave number in the regions of $0.2 \leq \xi \leq 2.2$ and $4.2 \leq \xi \leq 9.2$, the attenuation coefficient attains the value of 12.04 at $\xi = 3.2$ in the region of $2.2 \leq \xi \leq 4.2$; (ii) for the first symmetric mode, the magnitude of the attenuation coefficient for the G-L theory has negligible variation with wave number in the region of $0.2 \leq \xi \leq 6.2$, the attenuation coefficient attains the value of 51.31 at $\xi = 7.2$ in the region of $6.2 \leq \xi \leq 8.2$, the attenuation coefficient increases sharply to 157.9 as the wave number increases from 8.2 to 9.2; (iii) for the second symmetric mode, the magnitude of the attenuation coefficient for the G-L theory has negligible variation with wave number in the region of $0.2 \leq \xi \leq 5.2$, and the attenuation coefficient attains a peak value of 63.91 at $\xi = 7.2$ in the region of $5.2 \leq \xi \leq 9.2$; (iv) for the lowest symmetric mode, the magnitude of the attenuation coefficient for the L-S theory has negligible variation with wave number in the regions of $0.2 \leq \xi \leq 1.2$ and $3.2 \leq \xi \leq 9.2$, and the attenuation coefficient attains the highest peak value of 477.3 at $\xi = 2.2$ in the region of $1.2 \leq \xi \leq 3.2$; (v) for the first symmetric mode, the magnitude of the attenuation coefficient for the L-S theory has negligible variation with wave number in the regions of $0.2 \leq \xi \leq 2.2$ and $4.2 \leq \xi \leq 9.2$, and the attenuation coefficient attains a value of 11.66 at $\xi = 3.2$ in the region of $2.2 \leq \xi \leq 4.2$; and (vi) for the second symmetric mode, the magnitude of the attenuation coefficient for the L-S theory has negligible variation with wave number in the regions of $0.2 \leq \xi \leq 5.2$ and $7.2 \leq \xi \leq 9.2$, and the attenuation coefficient attains a value of 19.71 at $\xi = 6.2$ in the region of $5.2 \leq \xi \leq 7.2$.

From Fig. 4 it is noticed that (a) for the lowest skew-symmetric mode, the magnitude of the attenuation coefficient for the G-L theory have maxima up to 257.1 and 65.84 in the regions of $0.2 \leq \xi \leq 2.7$ at $\xi = 1.2$ and $2.7 \leq \xi \leq 6.2$ at $\xi = 4.2$, respectively, and the magnitude of the attenuation coefficient has negligible variation with wave number in the region of $6.2 \leq \xi \leq 9.2$; (b) for the first skew-symmetric mode, the magnitude of the attenuation coefficient for the G-L theory has negligible variation with wave number in the regions of $0.2 \leq \xi \leq 1.2$ and $5.2 \leq \xi \leq 9.2$, and the attenuation coefficient for the G-L theory attains values of 13.82 and 6.31 at $\xi = 2.2$ and $\xi = 3.2$, respectively, in the region of $1.2 \leq \xi \leq 3.2$, and the attenuation coefficient attains the highest maximum value of 295.9 at $\xi = 4.2$ in the region of $3.2 \leq \xi \leq 5.2$; (c) for the second skew-symmetric mode, the attenuation coefficient for the G-L theory has negligible variation with wave number in the regions of $0.2 \leq \xi \leq 5.2$ and $7.2 \leq \xi \leq 9.2$, and have maxima up to 7.296 in the region of $5.2 \leq \xi \leq 7.2$ at $\xi = 6.2$; (d) for the lowest skew-symmetric mode, the magnitude

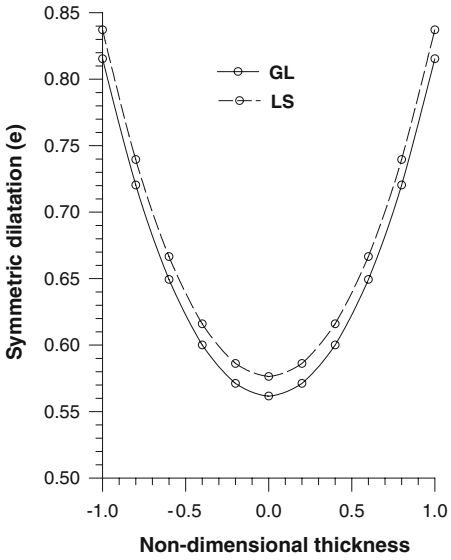

Fig. 5 Amplitude of symmetric dilatation (e) (for L-S theory, $\tau_1 = 0$, $\tau_0 > 0$, and $\eta_0 = 1$, and for G-L theory, $\tau_1 \geq \tau_0 > 0$, and $\eta_0 = 0$)

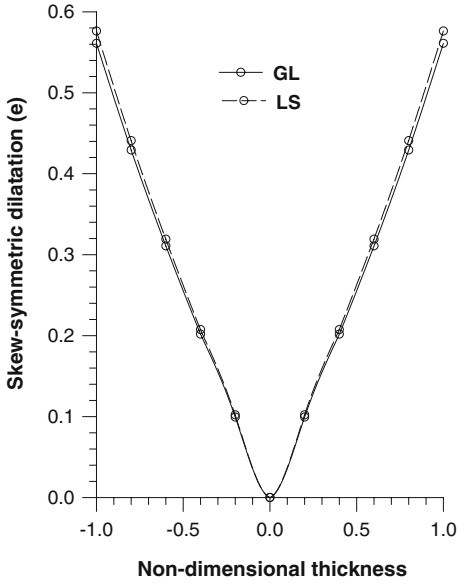

Fig. 6 Amplitude of skew-symmetric dilatation (e) (for L-S theory, $\tau_1 = 0$, $\tau_0 > 0$, and $\eta_0 = 1$, and for G-L theory, $\tau_1 \geq \tau_0 > 0$, and $\eta_0 = 0$)

of the attenuation coefficient for the L-S theory has a maximum value of 66.40 in the region of $0.2 \leq \xi \leq 3.2$ at $\xi = 0.2$, and the attenuation coefficient attains values of 29.97 and 24.97 at $\xi = 4.2$ and $\xi = 5.2$, respectively, in the region of $3.2 \leq \xi \leq 6.2$, and the magnitude of the attenuation coefficient has negligible variation with wave number in the region of $6.2 \leq \xi \leq 9.2$; (e) for the first skew-symmetric mode, the magnitude of the attenuation coefficient for the L-S theory has negligible variation with wave number in the regions of $0.2 \leq \xi \leq 1.2$ and $5.2 \leq \xi \leq 9.2$, and the

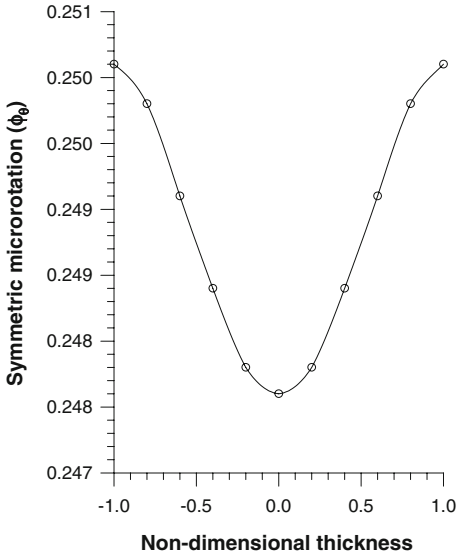

Fig. 7 Amplitude of symmetric microrotation (φ_θ) (for L-S theory, $\tau_1 = 0$, $\tau_0 > 0$, and $\eta_0 = 1$, and for G-L theory, $\tau_1 \geq \tau_0 > 0$, and $\eta_0 = 0$)

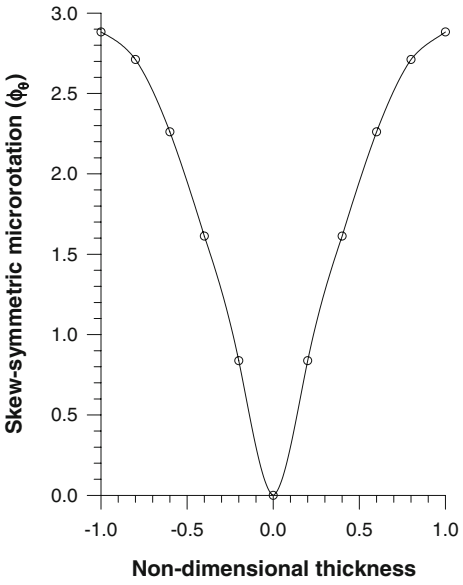

Fig. 8 Amplitude of skew-symmetric microrotation (φ_θ) (for L-S theory, $\tau_1 = 0$, $\tau_0 > 0$, and $\eta_0 = 1$, and for G-L theory, $\tau_1 \geq \tau_0 > 0$, and $\eta_0 = 0$)

attenuation coefficient attains a maximum value of 134.6 at $\xi = 4.2$ in the region of $3.2 \leq \xi \leq 5.2$; and (f) for the second skew-symmetric mode, the attenuation coefficient for the L-S theory has negligible variation with wave number in the region of $0.2 \leq \xi \leq 9.2$.

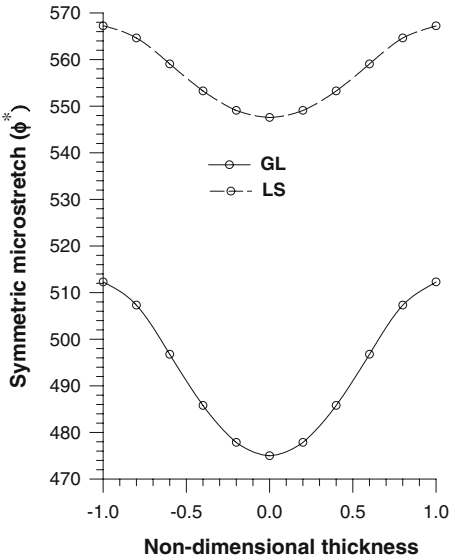

Fig. 9 Amplitude of symmetric microstretch (φ^*) (for L-S theory, $\tau_1 = 0$, $\tau_0 > 0$, and $\eta_0 = 1$, and for G-L theory, $\tau_1 \geq \tau_0 > 0$, and $\eta_0 = 0$)

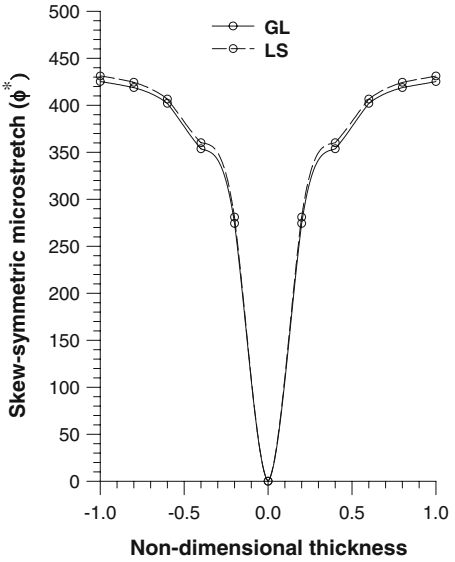

Fig. 10 Amplitude of skew-symmetric microstretch (φ^*) (for L-S theory, $\tau_1 = 0$, $\tau_0 > 0$, and $\eta_0 = 1$, and for G-L theory, $\tau_1 \geq \tau_0 > 0$, and $\eta_0 = 0$)

9.3 Amplitudes

Figures 5 and 6 depict the variations of symmetric and skew-symmetric amplitudes of the dilatation (e) in the context of L-S and G-L theories of thermoelasticity for a stress-free thermally insulated boundary. The dilatation (e) of the plate is a minimum at the center and a maximum at the surfaces for the symmetric mode and zero at the center and a maximum at the surfaces for the skew-symmetric mode as evident from Figs. 5 and 6, respectively. Figures 7–12 show the variations of symmetric and

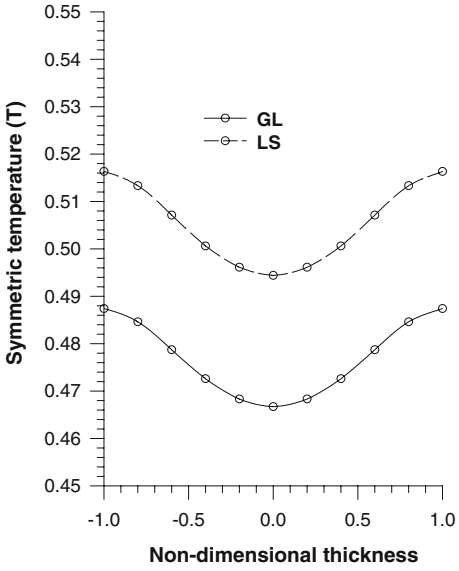

Fig. 11 Amplitude of symmetric temperature (T) (for L-S theory, $\tau_1 = 0$, $\tau_0 > 0$, and $\eta_0 = 1$, and for G-L theory, $\tau_1 \geq \tau_0 > 0$, and $\eta_0 = 0$)

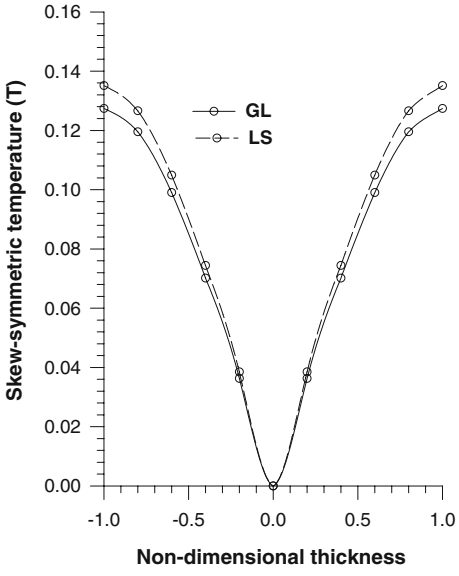

Fig. 12 Amplitude of skew-symmetric temperature (T) (for L-S theory, $\tau_1 = 0$, $\tau_0 > 0$, and $\eta_0 = 1$, and for G-L theory, $\tau_1 \geq \tau_0 > 0$, and $\eta_0 = 0$)

skew-symmetric amplitudes of microrotation (φ_θ), microstretch (φ^*), and the temperature distribution (T) in the context of L-S and G-L theories of thermoelasticity for a stress-free thermally insulated boundary. It is evident from Figs. 7–12 that the values of microrotation (φ_θ), microstretch (φ^*), and the temperature distribution (T) of the plate show minima at the center and maxima at the surfaces for the symmetric mode and zero at the center and maxima at the surfaces for the skew-symmetric mode. $(e)_{\text{sym}}$, $(e)_{\text{asym}}$, $(\varphi_\theta)_{\text{sym}}$, $(\varphi_\theta)_{\text{asym}}$, $(\varphi^*)_{\text{sym}}$, $(\varphi^*)_{\text{asym}}$, $(T)_{\text{sym}}$, and $(T)_{\text{asym}}$

correspond to the values of (e), (φ_θ), (φ^*), and (T) for symmetric and skew-symmetric modes, respectively. It is observed that the behavior and trend of variations of $(e)_{\text{sym}}$, $(\varphi_\theta)_{\text{sym}}$, $(\varphi^*)_{\text{sym}}$, and $(T)_{\text{sym}}$ are the same, whereas the behavior and trend of variations of $(e)_{\text{asym}}$, $(\varphi_\theta)_{\text{asym}}$, $(\varphi^*)_{\text{asym}}$, and $(T)_{\text{asym}}$ are similar. The values of the dilatation, microstretch, and temperature distribution of the plate for the case of the G-L theory are less in comparison to the L-S theory for symmetric and skew-symmetric modes. The values of the microrotation (φ_θ) of the plate are the same in the case of L-S and G-L theories of thermoelasticity for symmetric and skew-symmetric modes.

10 Conclusions

(i) The elastodynamic behavior of waves in a thermo-microstretch elastic homogeneous isotropic plate bordered with layers of inviscid liquid on both sides subjected to stress-free thermally insulated and isothermal conditions is investigated.
(ii) At the short-wavelength limit, the secular equations for symmetric and skew-symmetric wave modes reduce to the Rayleigh surface wave frequency equation.
(iii) The phase velocities of higher modes of propagation, symmetric, and skew-symmetric attain quite large values at a vanishing wave number which sharply decreases to become steady and asymptotic with increasing wave number.
(iv) The values of dilatation, microrotation, microstretch, and temperature distribution of the plate are minima at the center and maxima at the surfaces for the symmetric mode and zero at the center and maxima at the surfaces for the skew-symmetric mode.
(v) The values of the dilatation, microstretch, and temperature distribution of the plate in the case of the G-L theory are less in comparison to the L-S theory for symmetric and skew-symmetric modes.
(vi) The values of the microrotation of the plate are the same for both L-S and G-L theories of thermoelasticity for symmetric and skew-symmetric modes.

References

1. A.C. Eringen, *Micropolar Elastic Solids with Stretch* (Prof. Dr. Mustafa Inan Anisma, Ari Kitapevi Matbaasi, Istanbul, Turkey, 1971)
2. A.C. Eringen, Int. J. Eng. Sci. **28**, 1291 (1990)
3. A.C. Eringen, *Microcontinuum Field Theories I: Foundations and Solids* (Springer-Verlag, New York, 1999)
4. A.C. Eringen, Int. J. Eng. Sci. **28**, 133 (1990)
5. H. Lord, Y. Shulman, J. Mech. Phys. Solids **15**, 299 (1967)
6. A.E. Green, K.A. Lindsay, J. Elast. **2**, 1 (1972)
7. V.A. Schoch, Acoustica **2**, 1 (1952)
8. G. Kurtze, R.H. Bolt, Acoustica **9**, 238 (1959)
9. R.D. Watkins, W.H.B. Cooper, A.B. Gillespie, R.B. Pike, Ultrasonics **20**, 257 (1982)
10. J. Wu, Z. Zhu, J. Acoust. Soc. Am. **91**, 861 (1992)
11. Z. Zhu, J. Wu, J. Acoust. Soc. Am. **98**, 1057 (1995)
12. J.N. Sharma, V. Pathania, S.K. Gupta, Int. J. Eng. Sci. **41**, 1219 (2003)
13. J.N. Sharma, V. Pathania, S.K. Gupta, Int. J. Eng. Sci. **42**, 99 (2004)
14. H. Lamb, Philos. Trans. R. Soc. A **93**, 114 (1917)